AMERICAN SOCIETY FOR MICROBIOLOGY | Infection and Immunity

| Bacteriology | Full-Length Text

Connections between *Klebsiella pneumoniae* bloodstream dynamics and serotype-independent capsule properties

Emily L. Kinney,[1] Drew J. Stark,[1] Saroj Khadka,[1] Christine M. Tin,[2,3,4] Timothy W. Hand,[2,3,4,5] William Bain,[6,7] Laura A. Mike[1]

AUTHOR AFFILIATIONS See affiliation list on p. 15.

ABSTRACT *Klebsiella pneumoniae* bacteremia is a significant public health burden with a 26% mortality rate, which increases when the infecting isolate is multidrug resistant. An important virulence factor of *K. pneumoniae* is its capsule, the protective polysaccharide coat that surrounds the outer membrane and is made up of individual capsular polysaccharide (CPS) chains. The capsule can differ in composition, abundance, surface attachment, and length of the individual CPS chains. Long, uniform CPS chains are associated with a high level of mucoidy. Typically, mucoidy is produced by the hypervirulent *K. pneumoniae* (hvKp) pathotype, which is associated with invasive community-acquired infections. In contrast, the classical *K. pneumoniae* (cKp) pathotype tends to be less mucoid or non-mucoid and is associated with nosocomial infections and multidrug resistance. There are over 80 serotypes of *K. pneumoniae* capsule. Capsule swap experiments have begun to reveal the effect of serotype on virulence and immune interactions. Clinically, the K2 capsule serotype is a common serotype associated with neonatal bloodstream infections. Both cKp and hvKp can produce K2 capsule, but how K2-encoding cKp and hvKp strains differ in a bloodstream infection remains unknown. To fill this gap in knowledge, we characterized the surface properties of K2 serotype cKp and hvKp bloodstream infection isolates then tested the fitness of these strains in bloodstream infection-related *in vitro* and *in vivo* assays. Understanding how K2 cKp and hvKp strains differ in pathogenic potential provides further insights into how *K. pneumoniae* capsule properties influence bloodstream infection pathogenesis.

KEYWORDS *Klebsiella pneumoniae*, bacteremia, capsule, bloodstream infections, mucoidy, hmv, host-pathogen, siderophores, complement resistance, macrophages

Globally, *Klebsiella pneumoniae* is the third leading cause of antimicrobial resistance-related deaths (1). It is a gram-negative pathogen that infects a variety of host sites, including the urinary tract, lungs, and blood. *K. pneumoniae* bacteremia has a 26% mortality rate, which increases with antimicrobial resistance (2). According to the Child Health and Mortality Prevention Surveillance network, *K. pneumoniae* is implicated in 1 in 4 deaths among children under age 2 in low- and middle-income countries (3–5). It is also the primary cause of neonatal sepsis (6–8). There are two distinctly alarming pathotypes of *K. pneumoniae,* classical (cKp) and hypervirulent (hvKp). cKp strains are generally associated with nosocomial infections and multidrug resistance (9, 10). Meanwhile, hvKp strains are associated with community-acquired and invasive infections (11). Despite these observed pathogenic differences, both pathotypes can encode similar virulence properties.

The capsule is the protective polysaccharide coat that surrounds the outer membrane of *K. pneumoniae* and is composed of individual capsular polysaccharide (CPS) chains. The CPS can differ in serotype (capsule composition), abundance (total capsule synthesized), chain length (mode length of individual CPS chains), chain length diversity (range of CPS chain length), and attachment (outer membrane association).

Editor Andreas J. Bäumler, University of California Davis, Davis, California, USA

Address correspondence to Laura A. Mike, laura.mike@pitt.edu.

The authors declare no conflict of interest.

Received 17 November 2025
Accepted 5 December 2025
Published 29 January 2026

These nuanced capsular properties contribute to different physiological and pathogenic functions in bacteria (12). Compared to cKp, hvKp has been reported to exhibit increased capsule abundance, mucoidy, and other virulence factors linked with increased frequency of invasive infections (10, 13, 14). Recent work demonstrated that mucoidy is not driven by increased capsule abundance; rather, mucoidy is due to increased CPS chain length uniformity (15–17). While the presence of the capsule blocks complement-mediated killing, mucoidy blocks macrophage association (18–21).

There are over 80 different *K. pneumoniae* capsule serotypes, all with a different composition. However, most of the K-serotype diversity is observed in cKp as hvKp primarily produces K1 and K2 (14, 22–27). In recent years, elegant capsule swap experiments have begun to reveal the effect of individual serotypes on virulence, immune interactions, and phage dynamics (28–30). In a recent study by Huang et al., swapping the K2 capsule biosynthesis locus with either the K1 locus or a complemented K2 locus caused 100% mortality in mice, and all intravenous infections had high bacteremia (28). When the K2 capsule was replaced with the K3 or K23 serotype, the mice exhibited 100% survival, and intravenous infections had low bacteremia. Their study highlights the importance of considering the capsule serotype in *K. pneumoniae* studies. More broadly, studies comparing cKp and hvKp strains have typically focused on antibiotic resistance profiles, mucoid phenotype, or overall virulence (31–33). However, most of these comparisons do not control for capsule serotype. Since capsule serotype can significantly affect the outcome of an infection, including different serotypes when comparing cKp and hvKp could confound data interpretation (34). To overcome this limitation, we have compared virulence phenotypes of K2 serotype cKp and hvKp isolates since the K2 capsule serotype is prevalent in neonatal sepsis and community-acquired and hospital-acquired infections (6, 35, 36).

Here, we aimed to understand how K2 cKp and hvKp differ in their interaction with host defense mechanisms in the context of bloodstream infections. To assess the role of serotype-independent capsule properties in bacteremia, we studied nine K2 bloodstream isolates (cKp $N = 5$; hvKp $N = 3$) and one common K2 hvKp lab strain (ATCC 43816-derived, KPPR1) (Table 1). We quantified their capsule properties and fitness in conditions that mimic facets of bloodstream infection, specifically human serum survival, whole blood survival, host cell association, and dissemination from the bloodstream. Surprisingly, K2 cKp and K2 hvKp exhibited similar phenotypes in many assays. However, hvKp strains tend to be more mucoid, associate less with host cells, and achieve higher bacterial burdens in murine spleens and livers compared to cKp strains. These studies begin to reveal the serotype-independent role of specific capsule properties in a bloodstream infection.

RESULTS

K2 cKp and hvKp differ in mucoidy, not capsule abundance

Nine K2 bloodstream isolates and one common K2 hvKp lab strain (ATCC 43816-derived, KPPR1) were selected to investigate the relationship between serotype-independent capsule properties and bloodstream infection dynamics (Table 1). Based on whole-genome sequencing, all strains had at least two allele mismatches in the core genome and a range of differences in auxiliary genes, indicating that each is a unique strain (Table 1) (50). Strains were classified into pathotype based on the presence of the hypervirulent biomarkers: *rmp*, *rmpA2*, *peg-344*, *iuc*, and *iro* (37, 52). Since these genes are usually carried together on a hvKp plasmid, the presence of these genes predicts the presence of the hvKp plasmid (37). None of the cKp isolates had any of these biomarkers (Table 1). While hvKp1 had all five hypervirulent biomarkers, KPPR1, KPN165, and KPN49 had 3–4 of these hypervirulent biomarkers. Murine mortality from other studies has provided evidence that KPPR1, KPN49, and hvKp1 are hvKp (40, 53, 54). Thus, we designate KPN165 as a putative hvKp strain due to its lack of all five biomarkers and murine fatality data. KPPR1 has a low predicted virulence score due to the absence of aerobactin, but all other hvKp and putative hvKp strains had virulence scores of 4–5, and all cKp strains had

TABLE 1 Summary of K2 isolate genotypic properties[a,b]

Isolate	Reference	Pathotype	Sequence type	Life identification number (LIN) code	*wzi* Type	K Type	*rmp* locus	*rmpA2* locus	*peg-344*	Siderophore loci			Predicted virulence score	O locus	Predicted O type
										ybt locus	*iro* locus	*iuc* locus			
cKp83	(37)	cKp	25	0_0_388_1_49_0_0_0_0_0	*wzi72*	K2	–	–	–	*ybt14*	–	–	1	O1/O2v2	O1ab
KLP203	(38)	cKp	25	0_0_388_0_1_0_9_0_1_0	*wzi72*	K2	–	–	–	*ybt14*	–	–	1	O1/O2v2	O1ab
KLP679	(38)	cKp	25	0_0_388_0_1_0_9_0_28_0	*wzi72*	K2	–	–	–	*ybt14*	–	–	1	O1/O2v2	O2afg
Kp6984	(39)	cKp	14	0_0_1_1_71_0_0_0_0_0	*wzi2*	K2	–	–	–	–	–	–	0	O1/O2v1	O1ab
Kp11996	(39)	cKp	14	0_0_1_1_26_2_5_0_0_0	*wzi2*	K2	–	–	–	–	–	–	0	O1/O2v1	O1ab
KPPR1	(40–43)	hvKp	493	0_0_209_1_0_0_0_0_0_0	*wzi2*	K2	*rmp3*	–	Present	*ybt2*	*iro3* (truncated)	–	1	O1/O2v1	O1ab
KPN165	(44)	Putative hvKp	380	0_0_339_0_16_0_0_0_0_0	*wzi203*	K2	*rmp2*	–	Present	ybt14 (truncated)	iro2 (truncated)	*iuc2*	4	O1/O2v1	O1ab
hvKp1	(37, 45)	hvKp	86	0_0_395_0_13_1_0_0_0_0	*wzi2*	K2	*rmp1*	*rmpA2_6-60%*	Present	*ybt1-*	*iro1*	*iuc1*	4	O1/O2v1	O1ab
KPN49	(44)	hvKp	66	0_0_278_0_1_4_0_0_0_0	*wzi257*	K2	*rmp2*	–	Present	*ybt12*	*iro2*	*iuc2*	5	O1/O2v2	O1ab

[a]Pathogenwatch was used to predict the listed properties based on whole-genome sequencing data (46–49). The BIGSdb-Pasteur database was used to determine the life identification number (LIN) of the isolates (50, 51).
[b]–, the absence of a gene.

virulence scores of 0–1 (Table 1). Based on these analyses, we will henceforth collectively refer to KPPR1, KPN165, KPN49, and hvKp1 as hvKp strains, even though KPN165 is missing one hvKp biomarker and supporting LD_{50} data.

hvKp strains are canonically described as exhibiting increased levels of capsule, mucoidy, and siderophores compared to cKp strains. To test whether this distinction holds while controlling for the capsule serotype, we tested the bloodstream infection isolates (Table 1) for cell-associated CPS and cell-free extracellular polysaccharide (EPS) production (55). Unexpectedly, both cKp and hvKp isolates produce similar quantities of CPS and EPS (Fig. 1A and B). Although mean CPS abundance was the same between the pathotypes, the hvKp strain KPN49 produced more CPS than each cKp strain (Fig. S1A). We then quantified mucoidy using low-speed centrifugation (55). As expected, the cKp isolates display less mucoidy than hvKp (Fig. 1C). Notably, we also observed that one cKp strain, Kp11996, was as mucoid as hvKp strain KPN165 (Fig. S1C). Finally, the cell-associated CPS chain length distribution was examined by resolving CPS on a SDS-PAGE gel and visualizing the polysaccharides with Alcian blue followed by a silver stain (55). Prior work has shown that strains with high mucoidy produce a uniform band of CPS, while non-mucoid strains produce a diverse smear of CPS (15, 21, 56). All hvKp strains and the mucoid cKp strain, Kp11996, produce a uniform CPS band, whereas all the non-mucoid cKp strains produce a diverse CPS smear (Fig. 1D). Notably, the mucoid level quantified by a sedimentation assay predicted CPS chain length uniformity by SDS-PAGE, even for cKp strain Kp11996 (Fig. S1C; Fig. 1D). In addition to capsule characteristics, we quantified the amount of siderophores produced by each of the strains. Since the lab strain KPPR1 does not produce aerobactin, which accounts for the majority of siderophore production and is a defining feature of hvKp, this strain was excluded from the pathotype comparison for siderophore production (37, 57, 58). Likely due to the small number of strains, there was a numerically but not statistically significant difference in siderophore production between the two pathotypes (Fig. 1E). While KPN49 had similar levels of siderophores to the classical strains, hvKp1 and KPN165 produced 3.3-fold more siderophores than the classical strains (Fig. S1D).

K2 cKp and hvKp exhibit similar growth kinetics

To determine if growth properties could shape differences in cKp and hvKp pathogenesis, we assessed strain growth in two different media. Strains were cultured in LB or M9 minimal medium with 20% heat-inactivated serum (HI Serum) as the carbon source, and the OD_{600} was measured every 15 min to generate a growth curve (Fig. S2). The doubling time and area under the curve (AUC) were calculated from each growth curve to quantify the maximal growth rate and yield (Fig. S3). No significant differences between cKp and hvKp were detected in doubling time or AUC in either condition (Fig. 2). Therefore, any observed pathogenic differences are not likely due to growth differences.

K2 cKp and hvKp have comparable human serum resistance, but cKp has greater C3 deposition

An important part of the immune system in the bloodstream is the complement cascade. In *Streptococcus pneumoniae*, the capsule serotype is a factor in complement resistance (59). Since our strains are all K2, we assessed whether there was a significant difference between cKp and hvKp sensitivity to pooled human serum when capsule serotype is not a variable. cKp and hvKp survive similarly in human serum, but cKp exhibit a bimodal-like distribution (Fig. 3A). No killing was observed in HI Serum, which served as a control to confirm bacterial killing was complement-mediated (Fig. 3B). The data for the individual strains are shown in Fig. S4. Next, we considered whether complement deposition predicted serum resistance. Cleavage of complement component C3 leads to C3b deposition on the bacteria surface as an important precursor to the pathway ending in MAC formation. We measured C3b deposition using flow cytometry. Interestingly, despite no difference in complement resistance between the pathotypes (Fig. 3A), we

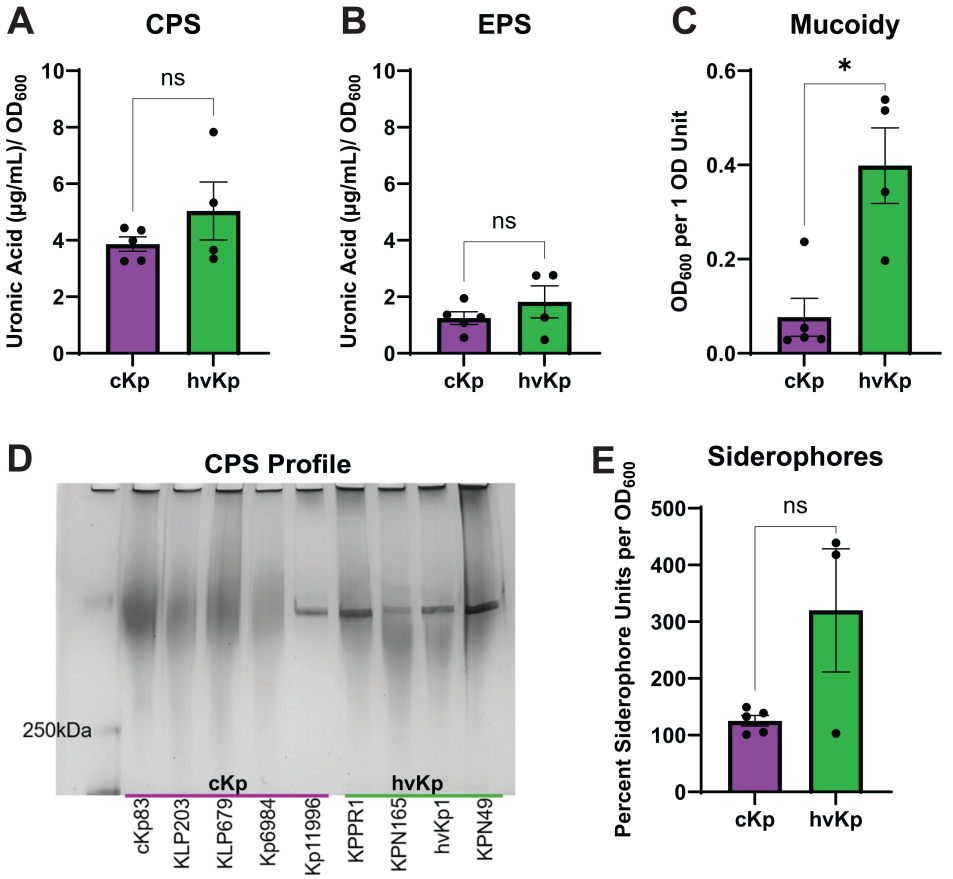

FIG 1 K2 cKp and hvKp strains differ in mucoidy, not capsule abundance. Capsule characteristics and siderophore quantity of K2 cKp and hvKp strains were determined. Uronic acid quantification measured (A) cell-associated CPS and (B) cell-free EPS abundance. (C) Sedimentation resistance was used to measure mucoidy. (D) Purified total CPS was resolved by a SDS-PAGE gel to visualize the CPS chain length distribution. Shown is a representative image from ≥3 independent experiments. (E) The colorimetric CAS assay was used to quantify siderophores. KPPR1 was excluded since it does not produce aerobactin. (A–C, E) Each data point represents the average of a single strain, where data were collected in triplicate ≥3 independent times. Individual data points for each strain are plotted in Fig. S1. Bars represent the mean, and error bars represent the standard error of the mean. To determine statistical significance, a normality test was first applied. A Mann-Whitney test was used in A, and an unpaired *t*-test was used in B, C, and E, where $*P < 0.05$ and ns = not significant.

observed higher C3b deposition on K2 cKp strains compared to the K2 hvKp strains (Fig. 3C). Histograms of C3b/iC3b-allophycocyanin (APC) staining are shown in Fig. S5.

Survival of K2 cKp and hvKp is similar in human blood, but cKp associate with macrophages more than hvKp

Given the lack of differences in human serum survival, we next assessed bacterial survival in whole human blood to consider whether another host factor in whole blood could influence cKp versus hvKp survival in the bloodstream. cKp and hvKp strains were incubated with human blood for either 1 or 1.5 h to compare survival patterns of the two pathotypes. cKp and hvKp exhibited similar survival at 1 or 1.5 h (Fig. 4A and B). However, there was a non-significant increase in bacteria between the two time points, indicating that after an initial period of bacterial death, *K. pneumoniae* can grow in human blood (Fig. 4A and B). Despite some donor-dependent trends in strain survival, no strain consistently survived better than other strains when data from the four donors were combined (Fig. S6A and B). Thus, cKp and hvKp survive comparably in blood.

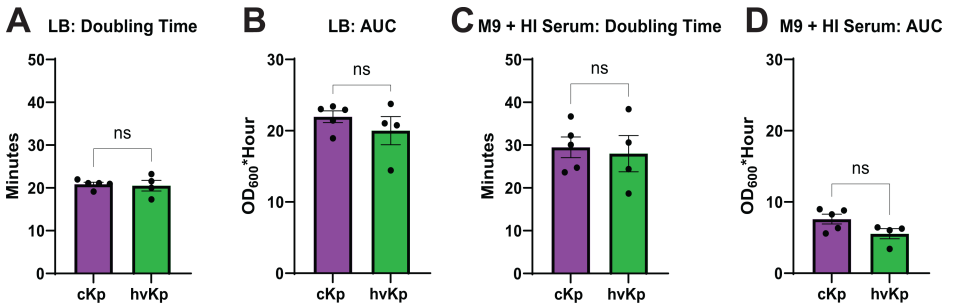

FIG 2 K2 cKp and hvKp exhibit similar growth properties. K2 cKp and hvKp strains were cultured in (A, B) LB or (C, D) M9 medium with 20% HI Serum as the carbon source. Growth was monitored by OD_{600} for 16 h. The (A, C) doubling time and (B, D) AUC were calculated from each growth curve. Each data point represents the average of a single strain, where data were collected in triplicate ≥3 independent times. Full growth curves are provided in Fig. S2, and individual data points for each strain are plotted in Fig. S3. Bars represent the mean, and error bars represent the standard error of the mean. To determine statistical significance, first, a test of normality was used. An unpaired *t*-test was used for A, B, and C, and a Mann-Whitney test was used for D, where ns = not significant.

To determine whether these pathotypes might differ in their interactions with host immune cells, we measured K2 cKp and hvKp association with iBMDMs. Due to antibiotic-resistance profiles, a gentamicin-protection assay could not be performed. Thus, the assay results include both intracellular and cell-bound bacteria. The K2 cKp isolates had a significantly higher association (26.3-fold) with the macrophages compared to the K2 hvKp isolates (Fig. 4C). Two cKp isolates, cKp83 and KLP203, had a significantly higher association than every hvKp isolate (Fig. S6C). This difference in macrophage binding suggests that reduced association of hvKp strains could contribute to the increased invasiveness of hvKp strains.

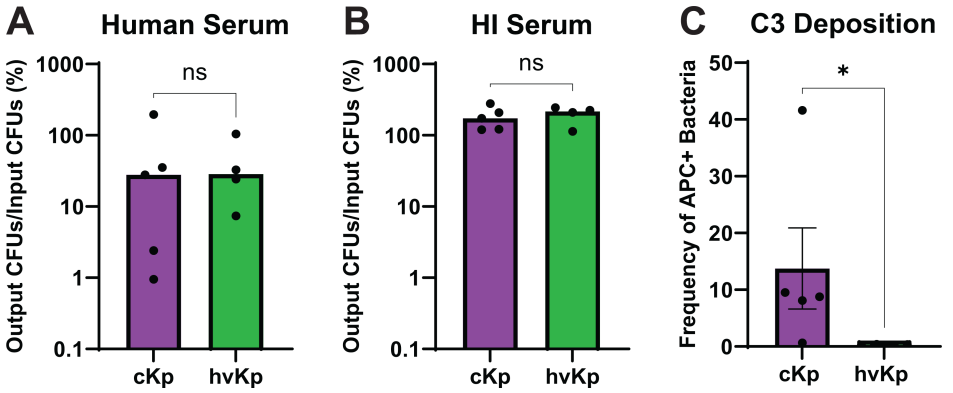

FIG 3 K2 cKp and hvKp have comparable human serum resistance, but cKp have greater C3 deposition. (A) K2 cKp and hvKp were incubated in 90% pooled human serum for 90 min. (B) HI serum was used as a control. Data are presented as the percentage of output colony-forming units (CFUs) divided by the input CFUs. Each data point represents the average of a single strain, where data were collected in triplicate ≥3 independent times. Each bar represents the median. Data for individual strains are presented in Fig. S4. (C) Strains were incubated with 10% human serum for 30 min and stained with SYTO BC green nucleic acid stain and C3b/iC3b-APC. The percentage of the bacterial population with APC stain is shown, where each data point represents the average of a single strain, collected ≥2 independent times. Each bar identifies the mean, and error bars represent the standard error of the mean. Individual APC histograms are shown in Fig. S5. To determine statistical significance, an unpaired *t*-test was used for A and B and a Mann-Whitney test for C, where ns = not significant and $*P < 0.05$.

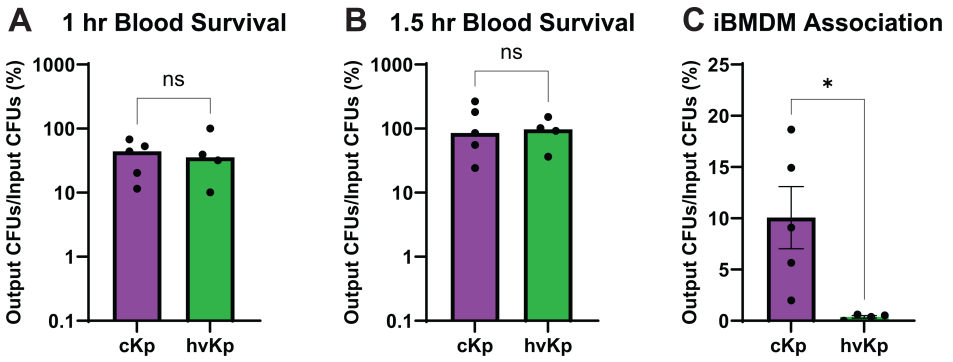

FIG 4 K2 cKp and hvKp survive similarly in human blood, but cKp associate with macrophages more than hvKp. K2 cKp and hvKp were incubated in 90% fresh whole human blood for (A, B) 60 or 90 min. (C) Strains were incubated with immortalized bone marrow-derived macrophages (iBMDMs) at a MOI of 10 for 2 h and then washed extensively prior to plating whole iBMDM lysates. For all graphs, data are presented as a percentage of the output CFUs divided by the input CFUs. Each data point represents the average of a single strain, where data were collected in triplicate ≥3 independent times. For A and B, each bar identifies the median. For C, the bar represents the mean, and the error bars represent the standard error of the mean. To determine statistical significance, an unpaired *t*-test (A,B) or Mann-Whitney test was used (C), where ns = not significant and **P* < 0.05.

K2 hvKp achieve higher bacterial spleen and liver burdens compared to cKp in a murine bloodstream infection model

Since K2 strains are prevalent in neonatal sepsis cases and all strains, except KPPR1, were isolated from bloodstream infections, we compared cKp and hvKp isolate dissemination patterns using a murine model of bacteremia (6, 35). Given the more invasive nature of hvKp, we expected to observe greater dissemination of hvKp compared to cKp. Mice were infected with 10^7 CFU of cKp (Kp6984 or cKp83) or hvKp (KPN165 or hvKp1) isolates via tail vein injection, and then blood-filtering organs were harvested after 24 h. Although no single strain achieved significantly higher tissue burdens compared to other individual strains (Fig. S6A through C), comparing combined data from both hvKp strains and both cKp strains detected significantly higher hvKp bacterial burdens in the spleen and liver (Fig. 5A through C). Additionally, while 100% of cKp-infected mice survived (*N* = 17/17) at the 24-h time point, only 80.8% of hvKp-infected mice (*N* = 21/26) survived, further supporting the enhanced virulence of hvKp strains *in vivo* (Fig. S6D). Furthermore, within the hvKp isolates, 23.5% of KPN165-infected mice did not survive compared to 11% of hvKp1-infected mice, indicating that KPN165 is as virulent or more virulent than hvKp1. Although we did not determine the LD_{50} of KPN165, these *in vivo* data support that KPN165 is likely a *bona fide* hvKp isolate. The decreased organ burden in cKp-infected mice suggests that cKp are less fit *in vivo*, or alternatively, that hvKp have an enhanced capacity for spleen and liver colonization.

Linear regressions reveal that some bacterial properties and host factors are linked

To determine whether any bacterial properties or host factors that we assessed interacted, we performed a correlation matrix between each factor. Our correlation analyses predict linkages between mucoidy and macrophage association (*P = 0.0004*), macrophage association and C3 deposition (*P = 0.0433*), and early-blood survival and late-blood survival *(P = 0.0083*) (Fig. 6). This does not necessarily mean that these properties depend on each other; for example, these properties could share related regulatory mechanisms or partition to a certain pathotype. While we primarily focused our analyses on capsule-related features, there may be other non-capsular factors affecting these phenotypes that we did not consider. One correlation that we expected to detect was between capsule abundance and human serum survival. Since the

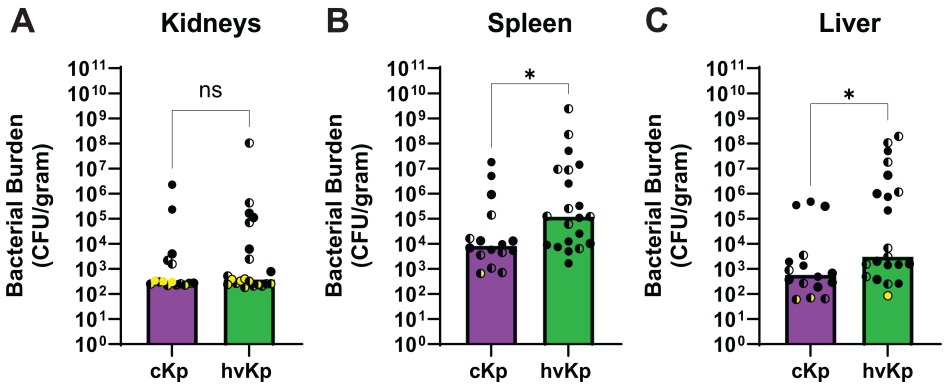

FIG 5 K2 hvKp achieve higher bacterial spleen and liver burdens compared to cKp in a murine bloodstream infection model. C57BL/6 mice were infected with 10^7 CFU of cKp (Kp6984 or cKp83) or hvKp (KPN165 or hvKp1) strains. After 24 h, mice were humanely euthanized, and bacterial burdens in the (A) kidneys, (B) livers, and (C) spleens were enumerated. Bars represent the median, and yellow dots represent points below the limit of detection. Each data point represents a single mouse, where half circles identify male mice and full circles identify female mice. Yellow dots represent points below the limit of detection. To determine statistical significance, a Mann-Whitney test was used, where $*P < 0.05$ and ns = not significant. Each strain was tested on at least 2 different days with at least 8 mice.

presence of the capsule has an established role in resisting complement-mediated killing, we hypothesized that increased capsule abundance would block the complement from reaching the cell surface (18–20). However, we did not detect any correlations between human serum survival and CPS or EPS abundance. In addition, we predicted that hvKp strains would withstand complement-mediated killing better than cKp strains, which could provide one mechanism for their invasive pathogenesis, but the hvKp isolates did not resist complement-mediated killing better than the cKp isolates (Fig. 3A). Moreover, the correlation matrix revealed no significant correlation between serum resistance and any quantified capsule characteristics (CPS abundance, EPS abundance, or mucoidy) (Fig. 6). Thus, when we only consider K2 serotype strains, neither the hvKp pathotype nor any capsule properties predicted serum resistance (Fig. 3 and 6). Notably, mucoidy was inversely correlated with iBMDM association, and both of these properties are significantly different between cKp and hvKp. This suggests that increased mucoidy and reduced iBMDM association could promote hvKp systemic dissemination, rather than increased CPS abundance or resistance to complement-mediated killing.

DISCUSSION

The cKp and hvKp pathotypes have been used to categorize *K. pneumoniae* and predict the pathogenic properties of a specific strain, but the vast genomic variation cannot be understated (60). This variation makes it risky to assume phenotypic homogeneity within each pathotype. Traditionally, the invasiveness of hvKp strains was attributed to elevated capsule abundance, mucoidy, and siderophore production (10, 13, 14, 61). However, most studies comparing these pathotypes have used isolates with a variety of capsule serotypes. We now know that capsule serotype itself alters the virulence, confounding these prior studies as hvKp strains tend to express the more immune-evasive capsule serotypes (K1 and K2) (28, 62). The experiments presented here reveal extensive phenotypic overlap between the two pathotypes. However, our study is limited by the number of isolates examined. Furthermore, the genomic diversity of the clinical isolates means that we cannot pinpoint the genetic differences underlying the observed phenotypic differences. Nonetheless, these data have identified several testable hypotheses for future studies. Compared to cKp, we observed that hvKp strains are more mucoid, have increased evasion of C3 deposition, associate less with macrophages, and achieve higher spleen and liver burdens, but exhibit no significant differences in CPS or EPS abundance, siderophore quantity, growth, serum resistance,

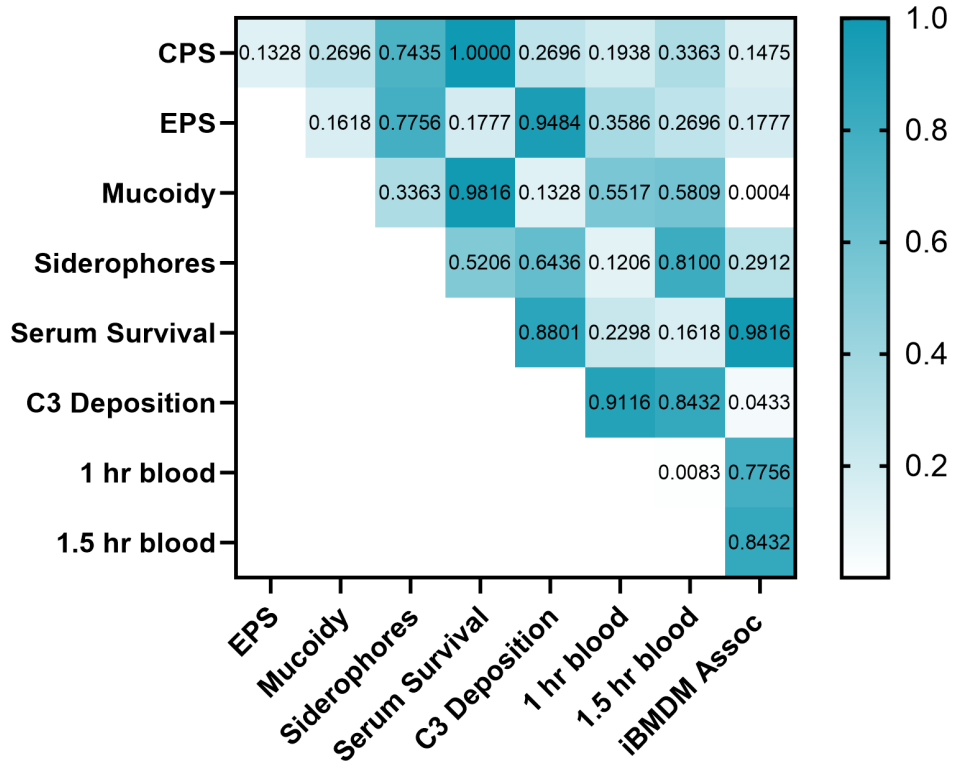

FIG 6 Correlations between bacterial properties and host interactions. A correlation matrix was used to compare relationships between quantified properties in Fig. 1, 3 and 4, using a nonparametric Spearman correlation and two-tailed *P*-values with a 95% CI. The *P*-values are displayed, and *P*-values below 0.05 were deemed significant.

or blood survival (Fig. 1 to 5). Even if a significant phenotypic difference was detected between cKp and hvKp, there was usually at least one strain whose phenotype matched the other pathotype. For example, the mucoidy of cKp strain Kp11996 mirrored the mucoidy of hvKp pathotype strains (Fig. S1C). However, this does not mean a single phenotype predicts strain virulence. In fact, prior work has proposed that a collection of biomarkers (*iucA*, *iroB*, *peg-344*, *rmpA*, and *rmpA2*) predict pathogenic differences between cKp and hvKp (63). Even though our data indicate that we cannot predict the specific behavior of an individual strain based solely on the pathotype, by controlling for serotype, our relatively small data set clarifies some relationships between surface characteristics and host interactions.

Our host assays tested bacterial interactions with cells and soluble bloodstream factors as phagocyte and complement activity are well-established immune components during *K. pneumoniae* bacteremia (64–66). We used pooled human serum to examine complement resistance and whole human blood to consider other soluble factors in blood that may control bacterial growth (67). The whole human blood assay captured both bacterial killing (1 hr) and bacterial growth (1.5 hr) (Fig. 4A and B). This allows us to hypothesize that while blood components initially control *K. pneumoniae* growth, some bacteria survive and can use blood as a nutrient source once immune components are depleted *ex vivo*. While the two pathotypes did not exhibit differences in human serum or human blood survival, hvKp had lower C3 deposition compared to cKp (Fig. 3 and 4; Fig. S5). This suggests that hvKp may evade complement-mediated killing by blocking C3 activation or deposition, while complement-resistant cKp may use an alternative mechanism. Thus, cKp and hvKp may employ different mechanisms to resist complement-mediated lysis, independent of the serotype. Since we did not see differences in complement-mediated killing between the pathotypes or any correla-

tions linking capsule characteristics with resistance to complement-mediated killing, we began investigating interactions with phagocytes.

To examine how these two pathotypes differ in phagocyte interactions, we measured cKp and hvKp binding to iBMDMs, an important precursor to phagocytosis. Phagocytosis was not measured here because the standard measure of phagocytosis is a gentamicin-protection assay, and some isolates are gentamicin-resistant. A previous study showed that serotype controls the ability of liver-resident macrophages (Kupffer cells) to capture *K. pneumoniae* (28). Since macrophages are an established line of defense against *K. pneumoniae* bloodstream infections, we used iBMDMs to model bacteria-host cell association (64, 68, 69). cKp exhibited a higher association with iBMDMs compared to hvKp, which inversely correlated with mucoidy, suggesting that mucoidy could shape bacterial-host immune cell binding (Fig. 4C and 6). This agrees with previous reports that hypermucoid strains associate less with macrophages and epithelial cells (16, 17, 70). Although the bacteria were not opsonized in the iBMDM association assay, opsonization increases cellular control of *K. pneumoniae* infections (71–73). The lack of C3b deposition on hvKp strains could further enhance the evasion of macrophage phagocytosis, increasing hvKp *in vivo* fitness. Additionally, C3b deposition and iBMDM association were correlated, suggesting that directly or indirectly related mechanisms may block bacterial interactions with these host elements. These results altogether led us to conclude that how cKp and hvKp interact with macrophages is a critical difference between the pathotypes. However, these phenotypes and their correlation could be due to non-capsular factors since the virulence properties are linked on the hvKp virulence plasmid (37). Further studies are needed to confirm the role of capsule properties in evading C3b deposition and iBMDM association.

Although the *ex vivo* assays provide some insights into how differences between K2 cKp and hvKp affect host interactions, we also wanted to examine the effect of pathotype differences during bloodstream dissemination. We selected two representative strains from each pathotype to minimize animal use. Within each pathotype, the selected strains have different levels of complement resistance and did not share the sequence type. All four strains have the same amount of CPS and EPS abundance, allowing us to remove that variable. We measured dissemination from the blood to the spleen, liver, and kidneys in a murine model. We selected these organs because they filter a large volume of blood. We observed inflammatory foci on the livers, likely abscesses, in both cKp- and hvKp-infected mice (Fig. S6E). Since this occurred in all strains, this suggests that the immune response to both pathotypes is similar in the liver. However, the two hvKp isolates had higher bacterial burdens in the spleen and liver than the two cKp isolates (Fig. 5). This suggests that the hvKp strains have a higher capacity to disseminate from the bloodstream than cKp, despite both pathotypes eliciting inflammatory foci in the livers. Alternatively, these data could indicate that the hvKp strains have increased capacity for growth or immune evasion in these sites (74). For example, low arginine abundance in the livers could optimize hvKp fitness factor expression (21). Nonetheless, from the bacterial burden and the overall survival of the mice, we can conclude that the hvKp isolates were more virulent than the cKp isolates tested in our murine model. Since the hvKp isolates used in the murine challenge both had elevated mucoidy and siderophore quantities compared to the cKp strains, we cannot conclude whether *in vivo* differences are due to mucoidy, siderophores, another factor, or a combination of these as each of these factors can contribute to hvKp *in vivo* fitness (57, 61, 75–77).

Our observation that cKp and hvKp exhibit similar survival in serum and blood, yet significant differences in iBMDM association and bacterial burden in the spleen and liver, may point to the importance of cell-mediated immunity in controlling *K. pneumoniae* bacteremia. Although complement is a major host factor in the bloodstream, our data indicate that direct serum killing may not be a major factor in the pathogenic potentials of cKp and hvKp in mice. For example, we observed that cKp isolate Kp6984, with low mucoidy and low human serum resistance, had similar bacterial organ burdens to the

cKp isolate with high human serum resistance, cKp83 (Fig. S6A through C). Our results either indicate that mouse serum may not limit *K. pneumoniae* growth as effectively as human serum or that human serum may not limit *K. pneumoniae* bloodstream survival. In support of the latter conclusion, a recent case study reported that selection for resistance to phagocytosis was observed more than resistance to complement in isolates collected from the bloodstream and during thoracoabdominal repair (78). Thus, the increased invasiveness of hvKp strains could be due to differences in immune cell association, likely due to both opsonized and non-opsonized processes, rather than direct killing by soluble factors.

An additional outcome of this study is the further evidence of the importance of the capsule serotype in *K. pneumoniae* infections. The overlapping phenotypes of K2 cKp and hvKp strains bolster evidence for the importance of serotype in *K. pneumoniae* pathogenesis. This agrees with capsule swap experiments that have started to uncover the effect of serotype on virulence, immune interactions, and phage dynamics (28–30). Studies have already begun to build on these data by developing vaccines for important capsule serotypes like K2 (79–81). Additionally, our study reveals questions for follow-up studies. We have shown that strains with similar lineages have some different phenotypes, raising questions regarding the genetic features underlying these phenotypic differences and the selective pressures driving phenotype emergence. One such phenotype is the difference in resistance to complement-mediated lysis between KLP203 and KLP679, despite aligning to the eighth bin in the LIN code (Table 1; Fig. S4A). Even if this serum survival difference is due to the O type or an auxiliary gene, understanding the mechanism driving the observed difference would expand our understanding of how *K. pneumoniae* resists complement-mediated lysis.

In summary, we have revealed that K2 cKp exhibit lower mucoidy, greater macrophage association, greater C3 deposition, and lower bacterial organ burdens after dissemination from the blood compared to K2 hvKp. However, we have also shown that there is a high degree of phenotypic overlap between these two pathotypes. These data offer insights into how K2 capsule characteristics of *K. pneumoniae* impact bacteremia pathogenesis and provide further evidence for the importance of controlling for the capsule serotype in *K. pneumoniae* pathogenesis work.

MATERIALS AND METHODS

Strain and culture conditions

Klebsiella pneumoniae isolates used in this study are reported in Table 1. Unless otherwise noted, strains were cultured in low-salt LB medium or on low-salt LB agar. Liquid cultures were incubated at 37°C for 15.5–16.5 h at 200 rpm, and plates were incubated at ambient temperatures or 37°C (46). The cKp and hvKp pathotypes were determined based upon the presence of the biomarkers *rmp*, *rmpA2*, *iro*, *iuc*, and *peg-344* (63). If a strain had all 5 biomarkers or previous murine fatality data, they were labeled as hvKp. If they had 3–4 biomarkers and no supporting murine fatality data from other labs, they were labeled putative hvKp. hvKp and putative hvKp isolates were analyzed together. The murine mortality from our infections with KPN165 supports that this strain is hvKp, whereas the murine mortality from others has shown that KPPR1, hvKp1, and KPN49 are hvKp (37, 40, 53, 54).

Uronic acid quantification

Capsule abundance was determined by uronic acid quantification, as previously described (16, 55, 82–84). To start, 250 µL of bacterial culture were added to 50 µL of either 1% Zwittergent 3-14 in 100 mM citric acid (to isolate total CPS) or distilled water (to isolate EPS). CPS samples were incubated at 50 °C for 20 min. All samples (CPS and EPS) were centrifuged at 17,000 × *g* for 5 min, and then 100 µL of the supernatant was added to 400 µL ice-cold absolute ethanol. Solutions were incubated on ice for 20 min

and then centrifuged at 17,000 × *g* for 5 min. Pellets were resuspended in 200 µL of water and then incubated at 37°C for 30 min. To each sample, 1.2 mL of 0.0125 M sodium tetraborate in sulfuric acid was added and then boiled at 100°C for 5 min and cooled on ice for 5 min. The absorbance of acid-treated samples at 520 nm (A_{520}) was measured. Subsequently, 10 µL of 0.3% 3-hydroxydiphenyl in 0.125 M sodium hydroxide was mixed into each sample, and the A_{520} was measured again. A glucuronic acid standard curve was used to determine the uronic acid amount in each sample. EPS was subtracted from total CPS to get cell-associated CPS. CPS and EPS levels were presented as uronic acid concentration per OD_{600}.

Sedimentation assay

Mucoidy was measured using sedimentation resistance, as in Khadka et al. (16, 55). The OD_{600} of bacterial cultures was measured and normalized to 1 OD_{600} unit in 1 mL. Then, the samples were subjected to a standard low-speed centrifugation (1,000 × *g* for 5 min), and the supernatant OD_{600} was measured. Mucoidy was plotted as the supernatant OD_{600} per 1 OD_{600} unit.

CPS chain length visualization

To analyze the CPS chain length mode and distribution, purified CPS samples were visualized using an SDS-PAGE gel, as previously described (15, 55, 56, 85). The bacterial cultures were normalized to 1.5 OD_{600}. Samples were centrifuged at 21,000 × *g* for 15 min, and then all of the supernatant, except for 50 µL (including the pellet), was removed. The remaining pellet was resuspended in 1 mL PBS. The resuspended pellet was centrifuged at 21,000 × *g* for 15 min, and then all but 250 µL was removed. A 50 µL aliquot of 1% Zwittergent 3-14 in 100 mM citric acid was added to the samples (5:1 sample:Zwittergent), followed by incubation at 50°C for 20 min. CPS samples were pelleted at 17,000 × *g* for 5 min, and then 100 µL of the supernatant was added to 400 µL ice-cold absolute ethanol. Solutions were incubated on ice for 20 min and then pelleted at 17,000 × *g* for 5 min. Pellets were rehydrated in 200 µL of water at 37°C for 30 min. Next, 75 µL of solubilized CPS samples were added to 25 µL of 4× SDS-gel loading dye, and then 20 µL of each sample was resolved on a 4%–15% Mini-PROTEAN TGX stain-free pre-cast gel (Bio-Rad) by applying 300 V for 4.5 h at 4°C. The gel was washed five times in ultra-pure water for 10 min, then stained with 0.1% Alcian blue in stain base solution (40% ethanol and 60% 20 mM sodium acetate, pH 4.75) for 1 h, and then the stain base solution was added to de-stain the gel overnight. The gel was stained using a Pierce Silver Stain Kit (ThermoFisher) and imaged on a Bio-Rad GelDoc.

CAS assay

Siderophores were quantified using the CAS Assay (86, 87). Cultures were grown in T medium while shaking for 18 h. Cultures were centrifuged at 9,614 × *g* for 5 min, and then 500 µL of the supernatant was mixed with 500 µL CAS reagent and 10 µL of the shuttle solution (0.2 M 5-sulfosalicyclic acid). OD_{630} was measured after 5 min. Percent siderophore units were defined as [(Ar-As)/Ar]100, where Ar is the absorbance of the buffer with the CAS reagent and the shuttle solution and As is the absorbance of the sample. Percent siderophore units were divided by the OD_{600} of each sample.

T medium was made using 6.8 g/L NaCl, 3.7 g/L KCl, 1.1 g/L NH_4Cl, 0.142 g/L Na_2SO_4, 0.00272 g/L KH_2PO_4, and 12.1 g/L tris(hydroxymethyl)aminomethane (88, 89). The pH of the solution was adjusted to 7.4. The solution was chelexed for 3 h at room temperature and then sterile-filtered. The solution was supplemented with 0.113 g/L anhydrous $CaCl_2$, 0.10 g/L $MgCl_2$ 6 H_2O, 1× vitamin solution, and 0.4% glucose. One liter of 100× vitamin solution is composed of 50 mL 0.02 M thiamine HCl, 50 mL 0.02 M calcium pantothenate, 50 mL 0.02 M *p*-aminobenzoic acid, 50 mL 0.02 M *p*-hydroxybenzoic acid, and 50 mL 0.02 M 2,3-dihydroxybenzoic acid.

The CAS reagent was made by first dissolving 0.0219 g HDTMA in 50 mL water. Separately, 1.5 mL 1 mM $FeCl_3$ 6 H_2O in 10 mM HCl and 7.5 mL of 2 mM CAS solution

were mixed. This solution was then slowly added to the HDTMA. In a separate beaker, 4.307 g piperazine was dissolved in 30 mL water, and then the pH was adjusted to 5.6. This solution was then added to the HDTMA/Fe/CAS solution. Then, the volume was brought to 100 mL with water.

Bioinformatics

Pathogenwatch software (version 23.4.0 https://pathogen.watch) was used to determine the sequence type, O locus, O type, and presence of the *rmp*, *rmpA2*, *iro*, and *iuc* loci from the genomic sequence of the bacterial strains (46–49). BLAST was used to determine the presence of *peg-344*. The genomic sequences were obtained from either the NCBI public database, requested from the strain source, or sequenced on the Illumina platform (SeqCoast) (Table 2). The BIGSdb-Pasteur database was used to determine the LIN of the isolates (50, 51).

Bacterial growth assay

Bacterial growth curves were generated following the protocol detailed by Pariseau et al. (46). Specifically, stationary-phase bacterial cultures were sub-cultured in LB and incubated for 1.5 h at 37°C, shaking at 200 rpm. The sub-cultured samples were diluted to 0.0001 OD_{600} in either LB or low-iron M9 minimal medium supplemented with $CaCl_2$, $MgSO_4$, and 20% HI human serum (Innovative Research). The samples were cultured with continuous shaking at 37°C, and the OD_{600} was measured every 15 min for 16 h using a microplate reader (Biotek Synergy HTX by Agilent).

Human serum survival

Bacterial survival in human serum was measured as described by Mike et al. (16). Strains were centrifuged at 16,249 × *g* for 10 min and then resuspended in sterile PBS. The resuspended samples were then diluted to an OD_{600} of 0.02. The diluted bacterial preparations were incubated in 90% pooled human serum (Innovative Research) or HI serum (inactivated at 58°C for 1 h) at 37°C for 90 min. Bacterial CFUs in the input and output samples were enumerated by serial dilution and plated on LB agar. Bacterial survival was presented as the percentage of input CFUs surviving after incubation.

C3 deposition

Complement deposition on the bacterial surface was measured using flow cytometry, as described by Bain et al. (73). Briefly, overnight bacterial cultures were sub-cultured (1:100) in LB. Once the sub-culture reached the log growth phase, the culture density was adjusted to 0.2 OD_{600} and then resuspended in GVB^o (ComplementTechnology #B103; no Mg or Ca). Bacteria (250 µL) were incubated with 25 µL MgEGTA and serum (Complement Tech; 50 µL normal human serum, 25 µL C3-depleted serum, or no serum) for 30 min at 37 °C. The reaction was quenched (750 µL cold, sterile PBS), pelleted (1,900 × *g* for 5 min), then washed twice by resuspending in 500 µL PBS, centrifuging, and then removing the supernatant. Each sample was resuspended in 100 µL 2% FBS in PBS, and then 50 µL was removed. Flow antibodies (2.5 µL ; 1:20 dilution per 10^6 cells) were added to the tubes: C3b/iC3b-APC (Biolegend 846106) and SYTO BC green nucleic acid stain (Invitrogen by Thermo Fisher Scientific S34855). The reaction was incubated at 4°C for 30 min and then washed twice with PBS (centrifuged at 1,900 × *g* for 5 min, supernatant removed, then resuspended in 500 µL PBS). Samples were analyzed on a Fortessa 7 cytometer (thresholds: 200 for FSC, 200 for SSC, and 300 for SYTO BC).

Human blood collection

Blood from healthy human donors was collected to use in the whole blood survival assay. Approximately 30 mL of blood were obtained through venipuncture after

TABLE 2 Genome accession number

Strain	SRA or SAMN
cKp83	SAMN51531023
KLP203	SAMN10435743
	SRS4051462
KLP679	SAMN38448741
	SRS19728011
Kp6984	SRR18486035
Kp11996	SRR19090175
KPN165	SAMN24009745
hvKp1	Chromosome: NZ_CP152338
	Plasmid: NZ_CP152339
KPN49	SAMN24009790

informed consent from the donor (CR19040346-008). The blood samples were collected in a sterile collection tube containing ACD-A as an anti-coagulant.

Survival in whole blood

Overnight bacterial cultures (1 mL) were centrifuged at 21,000 × *g* for 15 min and then resuspended in 1 mL sterile PBS, followed by dilution to an OD_{600} of 0.02. Then, 10 µL of the bacterial sample was incubated in 90 µL human blood (ACD-A tube) statically at 37 °C for 60 or 90 min. Bacterial CFUs in the input and output samples were enumerated by serial dilution and plated on LB agar. Bacterial survival and/or growth were presented as the percentage of input CFUs present after incubation.

Bone marrow-derived macrophage association assay

iBMDMs (BEI Resources NR-9456) were used to measure bacterial association to host cells (15). The macrophages were grown in a 24-well plate (n = 200,000 cells per well). Then, each well was infected with bacterial cells prepared in 1 mL Dulbecco's Modified Eagle Medium (DMEM) at an MOI of 10. The infected macrophages were briefly centrifuged down (54 × *g* for 5 min) to initiate cell contact. Then, the plate was incubated for 2 h, followed by washing with 1 mL sterile PBS three times. After washing, 1 mL 0.2% Triton-X-100 was added to each well for 5 min while shaking to lyse monocytes for bacterial release. The inocula (input) and macrophage lysates (output) were serially diluted and CFUs enumerated on LB agar. Bacterial association was presented as the percentage of output CFUs relative to input CFUs.

Murine bloodstream infection model

The *K. pneumoniae* murine bloodstream infection model used in this study was adapted from a previously described model and performed in adherence to humane animal handling recommendations and approved by the University of Pittsburgh Institutional Animal Care and Use Committee (protocol 24105753) (90). C57Bl/6 mice (7–8 weeks old) were procured from Charles River Laboratory (Ashland, OH, USA). The mice were injected with 10^7 bacteria via tail vein. After 24 h, the mice were humanely euthanized. The liver, spleen, and kidneys were collected then homogenized in sterile PBS. Bacterial burdens were determined by serially diluting the homogenized organs and then enumerating CFUs on LB agar. Bacterial burden was presented as the log-transformed CFUs divided by organ weight.

Statistics

All data, except for the murine bloodstream model and C3 deposition model, were collected on at least 3 different days. For these models, bacterial strains were used at least 2 different days. All statistical analyses were computed in Prism 10.3.1 (GraphPad

Software, La Jolla, CA, USA). Tests of normality were performed on all data. If normal, an unpaired *t*-test was used to compare data. If not normal, a Mann-Whitney test was used. For data with more than two comparisons, a one-way ANOVA was used if the data were normal, and a Kruskal-Wallis test was used if the data were not normal. Male and female mice and human blood donors were used to consider sex as a variable.

ACKNOWLEDGMENTS

The following reagent was obtained through BEI Resources, NIAID, NIH: Macrophage Cell Line Derived from Wild-Type Mice, NR-9456. We thank the Institut Pasteur teams for the curation and maintenance of BIGSdb-Pasteur databases at https://bigsdb.pasteur.fr/. We thank Drs. Tom Russo, Mike Bachman, Travis Kochan, Alan Hauser, Lora Pless, and Lee Harrison for the strains in this publication. We thank members of the Bain lab for their help with blood collection. We thank Mia Van Allen for her help with the CAS assay. We thank Nan Sheng for her help with flow cytometry. We thank members of the Mike lab and Program in Microbiology and Immunology at the University of Pittsburgh for critical feedback, especially Brooke Ryan, Grace Shepard, Zach Resko, Drs. Daria Van Tyne, John Alcorn, Prabir Ray, and Tera Levin.

Research reported in this publication was supported by the University of Pittsburgh College of Medicine and American Heart Association 23CDA1056712 (L.A.M.). This content is solely the responsibility of the authors and does not necessarily represent the official views of the American Heart Association.

AUTHOR AFFILIATIONS

[1]Department of Medicine, Division of Infectious Diseases, University of Pittsburgh, Pittsburgh, Pennsylvania, USA
[2]Department of Immunology, University of Pittsburgh, Pittsburgh, Pennsylvania, USA
[3]Department of Pediatrics, University of Pittsburgh, Pittsburgh, Pennsylvania, USA
[4]UPMC Children's Hospital of Pittsburgh, Pittsburgh, Pennsylvania, USA
[5]Institute of Infection, Immunity, and Inflammation in Children, UPMC Children's Hospital, Pittsburgh, Pennsylvania, USA
[6]Department of Medicine, Division of Pulmonary, Allergy, Critical Care, and Sleep Medicine, University of Pittsburgh, Pittsburgh, Pennsylvania, USA
[7]Veterans Affairs Pittsburgh Health System, Pittsburgh, Pennsylvania, USA

AUTHOR ORCIDs

Emily L. Kinney http://orcid.org/0000-0003-0269-2584
Drew J. Stark http://orcid.org/0000-0002-3185-2885
Saroj Khadka http://orcid.org/0000-0001-7533-7933
Christine M. Tin http://orcid.org/0000-0003-0190-0636
Timothy W. Hand http://orcid.org/0000-0002-2684-9462
William Bain http://orcid.org/0000-0001-8506-0552
Laura A. Mike http://orcid.org/0000-0002-3368-4184

AUTHOR CONTRIBUTIONS

Emily L. Kinney, Conceptualization, Data curation, Formal analysis, Investigation, Methodology, Visualization, Writing – original draft, Writing – review and editing | Drew J. Stark, Formal analysis, Investigation, Methodology, Writing – review and editing | Saroj Khadka, Formal analysis, Investigation, Writing – review and editing | Christine M. Tin, Investigation, Methodology | Timothy W. Hand, Methodology | William Bain, Methodology, Resources, Writing – review and editing | Laura A. Mike, Conceptualization, Data curation, Formal analysis, Funding acquisition, Methodology, Project administration, Supervision, Visualization, Writing – review and editing

DIRECT CONTRIBUTION

This article is a direct contribution from Laura A. Mike, a member of the *Infection and Immunity* Editorial Board, who arranged for and secured reviews by Thomas Russo, University at Buffalo, and Francois Lebreton, Walter Reed Army Institute of Research.

ADDITIONAL FILES

The following material is available online.

Supplemental Material

Supplemental figures (IAI00641-25-s0001.pdf). Fig. S1 to S7.

REFERENCES

1. Murray CJL, Ikuta KS, Sharara F, Swetschinski L, Robles Aguilar G, Gray A, Han C, Bisignano C, Rao P, Wool E, et al. 2022. Global burden of bacterial antimicrobial resistance in 2019: a systematic analysis. The Lancet 399:629–655. https://doi.org/10.1016/S0140-6736(21)02724-0
2. Holmes CL, Anderson MT, Mobley HLT, Bachman MA. 2021. Pathogenesis of Gram-negative bacteremia. Clin Microbiol Rev 34:e00234-20. https://doi.org/10.1128/CMR.00234-20
3. Taylor AW, Blau DM, Bassat Q, Onyango D, Kotloff KL, Arifeen SE, Mandomando I, Chawana R, Baillie VL, Akelo V, et al. 2020. Initial findings from a novel population-based child mortality surveillance approach: a descriptive study. Lancet Glob Health 8:e909–e919. https://doi.org/10.1016/S2214-109X(20)30205-9
4. Verani JR, Blau DM, Gurley ES, Akelo V, Assefa N, Baillie V, Bassat Q, Berhane M, Bunn J, Cossa ACA, et al. 2024. Child deaths caused by *Klebsiella pneumoniae* in sub-Saharan Africa and south Asia: a secondary analysis of Child Health and Mortality Prevention Surveillance (CHAMPS) data. Lancet Microbe 5:e131–e141. https://doi.org/10.1016/S2666-5247(23)00290-2
5. Bassat Q, Blau DM, Ogbuanu IU, Samura S, Kaluma E, Bassey I-A, Sow S, Keita AM, Tapia MD, Mehta A, et al. 2023. Causes of death among infants and children in the child health and mortality prevention surveillance (CHAMPS) network. JAMA Netw Open 6:e2322494. https://doi.org/10.1001/jamanetworkopen.2023.22494
6. Mukherjee S, Bhadury P, Mitra S, Naha S, Saha B, Dutta S, Basu S. 2023. Hypervirulent *Klebsiella pneumoniae* causing neonatal bloodstream infections: emergence of NDM-1-producing hypervirulent ST11-K2 and ST15-K54 strains possessing pLVPK-associated markers. Microbiol Spectr 11:e0412122. https://doi.org/10.1128/spectrum.04121-22
7. Viswanathan R, Singh AK, Basu S, Chatterjee S, Sardar S, Isaacs D. 2012. Multi-drug resistant gram negative bacilli causing early neonatal sepsis in India. Arch Dis Child Fetal Neonatal Ed 97:F182–F187. https://doi.org/10.1136/archdischild-2011-300097
8. Sands K, Carvalho MJ, Portal E, Thomson K, Dyer C, Akpulu C, Andrews R, Ferreira A, Gillespie D, Hender T, et al. 2021. Characterization of antimicrobial-resistant Gram-negative bacteria that cause neonatal sepsis in seven low- and middle-income countries. Nat Microbiol 6:512–523. https://doi.org/10.1038/s41564-021-00870-7
9. Moellering RC. 2010. NDM-1--a cause for worldwide concern. N Engl J Med 363:2377–2379. https://doi.org/10.1056/NEJMp1011715
10. Russo TA, Marr CM. 2019. Hypervirulent *Klebsiella pneumoniae*. Clin Microbiol Rev 32:e00001-19. https://doi.org/10.1128/CMR.00001-19
11. Holmes CL, Dailey KG, Hullahalli K, Wilcox AE, Mason S, Moricz BS, Unverdorben LV, Balazs GI, Waldor MK, Bachman MA. 2025. Patterns of *Klebsiella pneumoniae* bacteremic dissemination from the lung. Nat Commun 16:785. https://doi.org/10.1038/s41467-025-56095-3
12. Khadka S, Kinney EL, Ryan BE, Mike LA. 2025. Mechanisms governing bacterial capsular polysaccharide attachment and chain length. Ann N Y Acad Sci 1548:80–98. https://doi.org/10.1111/nyas.15364
13. Pomakova DK, Hsiao CB, Beanan JM, Olson R, MacDonald U, Keynan Y, Russo TA. 2012. Clinical and phenotypic differences between classic and hypervirulent *Klebsiella pneumonia*: an emerging and under-recognized pathogenic variant. Eur J Clin Microbiol Infect Dis 31:981–989. https://doi.org/10.1007/s10096-011-1396-6
14. Li W, Sun G, Yu Y, Li N, Chen M, Jin R, Jiao Y, Wu H. 2014. Increasing occurrence of antimicrobial-resistant hypervirulent (hypermucoviscous) *Klebsiella pneumoniae* isolates in China. Clin Infect Dis 58:225–232. https://doi.org/10.1093/cid/cit675
15. Khadka S, Ring BE, Walker RS, Krzeminski LR, Pariseau DA, Hathaway M, Mobley HLT, Mike LA. 2023. Urine-mediated suppression of *Klebsiella pneumoniae* mucoidy is counteracted by spontaneous Wzc variants altering capsule chain length. mSphere 8:e0028823. https://doi.org/10.1128/msphere.00288-23
16. Mike LA, Stark AJ, Forsyth VS, Vornhagen J, Smith SN, Bachman MA, Mobley HLT. 2021. A systematic analysis of hypermucoviscosity and capsule reveals distinct and overlapping genes that impact *Klebsiella pneumoniae* fitness. PLoS Pathog 17:e1009376. https://doi.org/10.1371/journal.ppat.1009376
17. Walker KA, Miner TA, Palacios M, Trzilova D, Frederick DR, Broberg CA, Sepúlveda VE, Quinn JD, Miller VL. 2019. A *Klebsiella pneumoniae* regulatory mutant has reduced capsule expression but retains hypermucoviscosity. mBio 10:e00089-19. https://doi.org/10.1128/mBio.00089-19
18. Short FL, Di Sario G, Reichmann NT, Kleanthous C, Parkhill J, Taylor PW. 2020. Genomic profiling reveals distinct routes to complement resistance in *Klebsiella pneumoniae*. Infect Immun 88:00043–20. https://doi.org/10.1128/IAI.00043-20
19. Doorduijn DJ, Rooijakkers SHM, van Schaik W, Bardoel BW. 2016. Complement resistance mechanisms of *Klebsiella pneumoniae*. Immunobiology 221:1102–1109. https://doi.org/10.1016/j.imbio.2016.06.014
20. Jensen TS, Opstrup KV, Christiansen G, Rasmussen PV, Thomsen ME, Justesen DL, Schønheyder HC, Lausen M, Birkelund S. 2020. Complement mediated *Klebsiella pneumoniae* capsule changes. Microbes Infect 22:19–30. https://doi.org/10.1016/j.micinf.2019.08.003
21. Ryan BE, Holmes CL, Stark DJ, Shepard GE, Mills EG, Khadka S, Van Tyne D, Bachman MA, Mike LA. 2025. Arginine regulates the mucoid phenotype of hypervirulent *Klebsiella pneumoniae*. Nat Commun 16:5875. https://doi.org/10.1038/s41467-025-61047-y
22. Lee C-R, Lee JH, Park KS, Jeon JH, Kim YB, Cha C-J, Jeong BC, Lee SH. 2017. Antimicrobial resistance of hypervirulent *Klebsiella pneumoniae*: epidemiology, hypervirulence-associated determinants, and resistance mechanisms. Front Cell Infect Microbiol 7:483. https://doi.org/10.3389/fcimb.2017.00483
23. Gu D, Dong N, Zheng Z, Lin D, Huang M, Wang L, Chan E-C, Shu L, Yu J, Zhang R, Chen S. 2018. A fatal outbreak of ST11 carbapenem-resistant hypervirulent *Klebsiella pneumoniae* in a Chinese hospital: a molecular epidemiological study. Lancet Infect Dis 18:37–46. https://doi.org/10.1016/S1473-3099(17)30489-9
24. Zhan L, Wang S, Guo Y, Jin Y, Duan J, Hao Z, Lv J, Qi X, Hu L, Chen L, Kreiswirth BN, Zhang R, Pan J, Wang L, Yu F. 2017. Outbreak by hypermucoviscous *Klebsiella pneumoniae* ST11 isolates with carbapenem resistance in a tertiary hospital in China. Front Cell Infect Microbiol 7:182. https://doi.org/10.3389/fcimb.2017.00182
25. Zhang Y, Zhao C, Wang Q, Wang X, Chen H, Li H, Zhang F, Li S, Wang R, Wang H. 2016. High prevalence of hypervirulent *Klebsiella pneumoniae* infection in China: geographic distribution, clinical characteristics, and antimicrobial resistance. Antimicrob Agents Chemother 60:6115–6120. https://doi.org/10.1128/AAC.01127-16
26. Liu YM, Li BB, Zhang YY, Zhang W, Shen H, Li H, Cao B. 2014. Clinical and molecular characteristics of emerging hypervirulent *Klebsiella*

pneumoniae bloodstream infections in mainland China. Antimicrob Agents Chemother 58:5379–5385. https://doi.org/10.1128/AAC.02523-14
27. Lee IR, Molton JS, Wyres KL, Gorrie C, Wong J, Hoh CH, Teo J, Kalimuddin S, Lye DC, Archuleta S, Holt KE, Gan Y-H. 2016. Differential host susceptibility and bacterial virulence factors driving Klebsiella liver abscess in an ethnically diverse population. Sci Rep 6:29316. https://doi.org/10.1038/srep29316
28. Huang X, Li X, An H, Wang J, Ding M, Wang L, Li L, Ji Q, Qu F, Wang H, Xu Y, Lu X, He Y, Zhang J-R. 2022. Capsule type defines the capability of *Klebsiella pneumoniae* in evading Kupffer cell capture in the liver. PLoS Pathog 18:e1010693. https://doi.org/10.1371/journal.ppat.1010693
29. Kabha K, Nissimov L, Athamna A, Keisari Y, Parolis H, Parolis LA, Grue RM, Schlepper-Schafer J, Ezekowitz AR, Ohman DE. 1995. Relationships among capsular structure, phagocytosis, and mouse virulence in *Klebsiella pneumoniae*. Infect Immun 63:847–852. https://doi.org/10.1128/iai.63.3.847-852.1995
30. Haudiquet M, Le Bris J, Nucci A, Bonnin RA, Domingo-Calap P, Rocha EPC, Rendueles O. 2024. Capsules and their traits shape phage susceptibility and plasmid conjugation efficiency. Nat Commun 15:2032. https://doi.org/10.1038/s41467-024-46147-5
31. Fursova AD, Fursov MV, Astashkin EI, Novikova TS, Fedyukina GN, Kislichkina AA, Alexandrova IA, Ershova ON, Dyatlov IA, Fursova NK. 2022. Early response of antimicrobial resistance and virulence genes expression in classical, hypervirulent, and hybrid hvKp-MDR *Klebsiella pneumoniae* on antimicrobial stress. Antibiotics (Basel) 11:7. https://doi.org/10.3390/antibiotics11010007
32. Wu H, Li D, Zhou H, Sun Y, Guo L, Shen D. 2017. Bacteremia and other body site infection caused by hypervirulent and classic *Klebsiella pneumoniae*. Microb Pathog 104:254–262. https://doi.org/10.1016/j.micpath.2017.01.049
33. Chen D, Zhang Y, Wu J, Li J, Chen H, Zhang X, Hu X, Chen F, Yu R. 2022. Analysis of hypervirulent *Klebsiella pneumoniae* and classic *Klebsiella pneumoniae* infections in a Chinese hospital. J Appl Microbiol 132:3883–3890. https://doi.org/10.1111/jam.15476
34. Zhuo X, Lei Z, Pu D, Wu Y, Zhao J, Cao B. 2025. Hypervirulent *Klebsiella pneumoniae* have better clinical outcomes than classical *Klebsiella pneumoniae* for lower respiratory tract infection patients. BMC Microbiol 25:40. https://doi.org/10.1186/s12866-024-03726-2
35. Stanton TD, Keegan SP, Abdulahi JA, Amulele AV, Bates M, Heinz E, Hooda Y, Hu W, Jain K, Kanwar S, et al. 2025. Distribution of capsule and O types in *Klebsiella pneumoniae* causing neonatal sepsis in Africa and South Asia: meta-analysis of genome-predicted serotype prevalence and potential vaccine coverage. medRxiv. https://doi.org/10.1101/2025.06.28.25330253:2025.06.28.25330253
36. Yu VL, Hansen DS, Ko WC, Sagnimeni A, Klugman KP, von Gottberg A, Goossens H, Wagener MM, Benedi VJ, International Klebseilla Study Group. 2007. Virulence characteristics of *Klebsiella* and clinical manifestations of *K. pneumoniae* bloodstream infections. Emerg Infect Dis 13:986–993. https://doi.org/10.3201/eid1307.070187
37. Russo TA, Olson R, Fang C-T, Stoesser N, Miller M, MacDonald U, Hutson A, Barker JH, La Hoz RM, Johnson JR. 2018. Identification of biomarkers for differentiation of hypervirulent *Klebsiella pneumoniae* from classical *K. pneumoniae*. J Clin Microbiol 56:e00776-18. https://doi.org/10.1128/JCM.00776-18
38. Sundermann AJ, Chen J, Kumar P, Ayres AM, Cho ST, Ezeonwuka C, Griffith MP, Miller JK, Mustapha MM, Pasculle AW, Saul MI, Shutt KA, Srinivasa V, Waggle K, Snyder DJ, Cooper VS, Van Tyne D, Snyder GM, Marsh JW, Dubrawski A, Roberts MS, Harrison LH. 2022. Whole-genome sequencing surveillance and machine learning of the electronic health record for enhanced healthcare outbreak detection. Clin Infect Dis 75:476–482. https://doi.org/10.1093/cid/ciab946
39. Vornhagen J, Roberts EK, Unverdorben L, Mason S, Patel A, Crawford R, Holmes CL, Sun Y, Teodorescu A, Snitkin ES, Zhao L, Simner PJ, Tamma PD, Rao K, Kaye KS, Bachman MA. 2022. Combined comparative genomics and clinical modeling reveals plasmid-encoded genes are independently associated with *Klebsiella* infection. Nat Commun 13:4459. https://doi.org/10.1038/s41467-022-31990-1
40. Broberg CA, Wu W, Cavalcoli JD, Miller VL, Bachman MA. 2014. Complete genome sequence of *Klebsiella pneumoniae* strain ATCC 43816 KPPR1, a rifampin-resistant mutant commonly used in animal, genetic, and molecular biology studies. Genome Announc 2:e00924-14. https://doi.org/10.1128/genomeA.00924-14
41. Bakker-Woudenberg IA, van den Berg JC, Vree TB, Baars AM, Michel MF. 1985. Relevance of serum protein binding of cefoxitin and cefazolin to their activities against *Klebsiella pneumoniae* pneumonia in rats. Antimicrob Agents Chemother 28:654–659. https://doi.org/10.1128/AAC.28.5.654
42. Roosendaal R, Bakker-Woudenberg IA, van den Berg JC, Michel MF. 1985. Therapeutic efficacy of continuous versus intermittent administration of ceftazidime in an experimental *Klebsiella pneumoniae* pneumonia in rats. J Infect Dis 152:373–378. https://doi.org/10.1093/infdis/152.2.373
43. Lawlor MS, Hsu J, Rick PD, Miller VL. 2005. Identification of *Klebsiella pneumoniae* virulence determinants using an intranasal infection model. Mol Microbiol 58:1054–1073. https://doi.org/10.1111/j.1365-2958.2005.04918.x
44. Kochan TJ, Nozick SH, Valdes A, Mitra SD, Cheung BH, Lebrun-Corbin M, Medernach RL, Vessely MB, Mills JO, Axline CMR, Nelson JA, VanGosen EM, Ward TJ, Ozer EA, van Duin D, Chen L, Kreiswirth BN, Long SW, Musser JM, Bulman ZP, Wunderink RG, Hauser AR. 2023. *Klebsiella pneumoniae* clinical isolates with features of both multidrug-resistance and hypervirulence have unexpectedly low virulence. Nat Commun 14:7962. https://doi.org/10.1038/s41467-023-43802-1
45. Bulger J, MacDonald U, Olson R, Beanan J, Russo TA. 2017. Metabolite transporter PEG344 is required for full virulence of hypervirulent *Klebsiella pneumoniae* strain hvKP1 after pulmonary but not subcutaneous challenge. Infect Immun 85:00093–17. https://doi.org/10.1128/IAI.00093-17
46. Pariseau DA, Ring BE, Khadka S, Mike LA. 2024. Cultivation and genomic DNA extraction of *Klebsiella pneumoniae*. Curr Protoc 4:e932. https://doi.org/10.1002/cpz1.932
47. Pathogenwatch. A global platform for genomic surveillance. Available from: https://pathogen.watch. Retrieved 20 Jun 2025.
48. Wyres KL, Wick RR, Gorrie C, Jenney A, Follador R, Thomson NR, Holt KE. 2016. Identification of *Klebsiella* capsule synthesis loci from whole genome data. Microb Genom 2:e000102. https://doi.org/10.1099/mgen.0.000102
49. Argimón S, David S, Underwood A, Abrudan M, Wheeler NE, Kekre M, Abudahab K, Yeats CA, Goater R, Taylor B, Harste H, Muddyman D, Feil EJ, Brisse S, Holt K, Donado-Godoy P, Ravikumar KL, Okeke IN, Carlos C, Aanensen DM. 2021. Rapid genomic characterization and global surveillance of *Klebsiella* using pathogenwatch. Clinical Infectious Diseases. https://doi.org/10.1101/2021.06.22.448967
50. Hennart M, Guglielmini J, Bridel S, Maiden MCJ, Jolley KA, Criscuolo A, Brisse S. 2022. A dual barcoding approach to bacterial strain nomenclature: genomic taxonomy of *Klebsiella pneumoniae* strains. Mol Biol Evol 39:msac135. https://doi.org/10.1093/molbev/msac135
51. Bialek-Davenet S, Criscuolo A, Ailloud F, Passet V, Jones L, Delannoy-Vieillard AS, Garin B, Le Hello S, Arlet G, Nicolas-Chanoine MH, Decré D, Brisse S. 2014. Genomic definition of hypervirulent and multidrug-resistant *Klebsiella pneumoniae* clonal groups. Emerg Infect Dis 20:1812–1820. https://doi.org/10.3201/eid2011.140206
52. Russo TA, MacDonald U, Hassan S, Camanzo E, LeBreton F, Corey B, McGann P. 2021. An assessment of siderophore production, mucoviscosity, and mouse infection models for defining the virulence spectrum of hypervirulent *Klebsiella pneumoniae*. mSphere 6:e00045-21. https://doi.org/10.1128/mSphere.00045-21
53. Kochan TJ, Nozick SH, Medernach RL, Cheung BH, Gatesy SWM, Lebrun-Corbin M, Mitra SD, Khalatyan N, Krapp F, Qi C, Ozer EA, Hauser AR. 2022. Genomic surveillance for multidrug-resistant or hypervirulent *Klebsiella pneumoniae* among United States bloodstream isolates. BMC Infect Dis 22:603. https://doi.org/10.1186/s12879-022-07558-1
54. Lawlor MS, Handley SA, Miller VL. 2006. Comparison of the host responses to wild-type and *cpsB* mutant *Klebsiella pneumoniae* infections. Infect Immun 74:5402–5407. https://doi.org/10.1128/IAI.00244-06
55. Khadka S, Ring BE, Pariseau DA, Mike LA. 2023. Characterization of *Klebsiella pneumoniae* extracellular polysaccharides. Curr Protoc 3:e937. https://doi.org/10.1002/cpz1.937
56. Ovchinnikova OG, Treat LP, Teelucksingh T, Clarke BR, Miner TA, Whitfield C, Walker KA, Miller VL. 2023. Hypermucoviscosity regulator RmpD interacts with Wzc and controls capsular polysaccharide chain length. mBio 14:e0080023. https://doi.org/10.1128/mbio.00800-23
57. Russo TA, Olson R, Macdonald U, Metzger D, Maltese LM, Drake EJ, Gulick AM. 2014. Aerobactin mediates virulence and accounts for increased siderophore production under iron-limiting conditions by hypervirulent

(hypermucoviscous) *Klebsiella pneumoniae*. Infect Immun 82:2356–2367. https://doi.org/10.1128/IAI.01667-13
58. Russo TA, Olson R, MacDonald U, Beanan J, Davidson BA. 2015. Aerobactin, but not yersiniabactin, salmochelin, or enterobactin, enables the growth/survival of hypervirulent (hypermucoviscous) *Klebsiella pneumoniae ex vivo* and *in vivo*. Infect Immun 83:3325–3333. https://doi.org/10.1128/IAI.00430-15
59. Melin M, Trzciński K, Meri S, Käyhty H, Väkeväinen M. 2010. The capsular serotype of *Streptococcus pneumoniae* is more important than the genetic background for resistance to complement. Infect Immun 78:5262–5270. https://doi.org/10.1128/IAI.00740-10
60. Holt KE, Wertheim H, Zadoks RN, Baker S, Whitehouse CA, Dance D, Jenney A, Connor TR, Hsu LY, Severin J, et al. 2015. Genomic analysis of diversity, population structure, virulence, and antimicrobial resistance in *Klebsiella pneumoniae*, an urgent threat to public health. Proc Natl Acad Sci USA 112:E3574–E3581. https://doi.org/10.1073/pnas.1501049112
61. Paczosa MK, Mecsas J. 2016. *Klebsiella pneumoniae*: going on the offense with a strong defense. Microbiol Mol Biol Rev 80:629–661. https://doi.org/10.1128/MMBR.00078-15
62. Le Bris J, Varet H, Rocha EPC, Rendueles O. 2025. Serotype swapping in *Klebsiella* spp. by plug-and-play. bioRxiv. https://doi.org/10.1101/2025.08.29.672822:2025.08.29.672822
63. Russo TA, Alvarado CL, Davies CJ, Drayer ZJ, Carlino-MacDonald U, Hutson A, Luo TL, Martin MJ, Corey BW, Moser KA, Rasheed JK, Halpin AL, McGann PT, Lebreton F. 2024. Differentiation of hypervirulent and classical *Klebsiella pneumoniae* with acquired drug resistance. MBio 15:e0286723. https://doi.org/10.1128/mbio.02867-23
64. Broug-Holub E, Toews GB, van Iwaarden JF, Strieter RM, Kunkel SL, Paine R 3rd, Standiford TJ. 1997. Alveolar macrophages are required for protective pulmonary defenses in murine *Klebsiella pneumonia*: elimination of alveolar macrophages increases neutrophil recruitment but decreases bacterial clearance and survival. Infect Immun 65:1139–1146. https://doi.org/10.1128/iai.65.4.1139-1146.1997
65. Bain W, Li H, van der Geest R, Moore SR, Olonisakin TF, Ahn B, Papke E, Moghbeli K, DeSensi R, Rapport S, Saul M, Hulver M, Xiong Z, Mallampalli RK, Ray P, Morris A, Ma L, Doi Y, Zhang Y, Kitsios GD, Kulkarni HS, McVerry BJ, Ferreira VP, Nouraie M, Lee JS. 2020. Increased alternative complement pathway function and improved survival during critical illness. Am J Respir Crit Care Med 202:230–240. https://doi.org/10.1164/rccm.201910-2083OC
66. DeLeo FR, Kobayashi SD, Porter AR, Freedman B, Dorward DW, Chen L, Kreiswirth BN. 2017. Survival of carbapenem-resistant *Klebsiella pneumoniae* sequence type 258 in human blood. Antimicrob Agents Chemother 61:02533–16. https://doi.org/10.1128/AAC.02533-16
67. Gautam I, Huss CW, Storad ZA, Krebs M, Bassiouni O, Ramesh R, Wuescher LM, Worth RG. 2023. Activated platelets mediate monocyte killing of *Klebsiella pneumoniae*. Infect Immun 91:e0055622. https://doi.org/10.1128/iai.00556-22
68. Wanford JJ, Hames RG, Carreno D, Jasiunaite Z, Chung WY, Arena F, Di Pilato V, Straatman K, West K, Farzand R, Pizza M, Martinez-Pomares L, Andrew PW, Moxon ER, Dennison AR, Rossolini GM, Oggioni MR. 2021. Interaction of *Klebsiella pneumoniae* with tissue macrophages in a mouse infection model and ex-vivo pig organ perfusions: an exploratory investigation. Lancet Microbe 2:e695–e703. https://doi.org/10.1016/S2666-5247(21)00195-6
69. Li Y, Li X, Wu W, Liu P, Liu J, Jiang H, Deng L, Ni C, Wu X, Zhao Y, Ren J. 2025. Insights into the roles of macrophages in *Klebsiella pneumoniae* infections: a comprehensive review. Cell Mol Biol Lett 30:34. https://doi.org/10.1186/s11658-025-00717-7
70. Walker KA, Treat LP, Sepúlveda VE, Miller VL. 2020. The small protein RmpD drives hypermucoviscosity in *Klebsiella pneumoniae*. mBio 11:e01750-20. https://doi.org/10.1128/mBio.01750-20
71. Kostina E, Ofek I, Crouch E, Friedman R, Sirota L, Klinger G, Sahly H, Keisari Y. 2005. Noncapsulated *Klebsiella pneumoniae* bearing mannose-containing O antigens is rapidly eradicated from mouse lung and triggers cytokine production by macrophages following opsonization with surfactant protein D. Infect Immun 73:8282–8290. https://doi.org/10.1128/IAI.73.12.8282-8290.2005
72. Valencia-Bacca JD, Jennings-Gee JE, Nutter NA, Adams-Sims AE, Hegarty AA, Didier HL, Ammar Zafar M, Haas KM. 2025. Divergent roles for complement components C3 and C4 in controlling *Klebsiella pneumoniae* gut colonization and systemic dissemination. bioRxiv. https://doi.org/10.1101/2025.10.09.681492:2025.10.09.681492
73. Bain W, Ahn B, Peñaloza HF, McElheny CL, Tolman N, van der Geest R, Gonzalez-Ferrer S, Chen N, An X, Hosuru R, et al. 2024. *In vivo* evolution of a *Klebsiella pneumoniae* capsule defect with wcaJ mutation promotes complement-mediated opsonophagocytosis during recurrent infection. J Infect Dis 230:209–220. https://doi.org/10.1093/infdis/jiae003
74. Bray AS, Broberg CA, Hudson AW, Wu W, Nagpal RK, Islam M, Valencia-Bacca JD, Shahid F, Hernandez GE, Nutter NA, Walker KA, Bennett EF, Young TM, Barnes AJ, Ornelles DA, Miller VL, Zafar MA. 2025. *Klebsiella pneumoniae* employs a type VI secretion system to overcome microbiota-mediated colonization resistance. Nat Commun 16:940. https://doi.org/10.1038/s41467-025-56309-8
75. Holden VI, Breen P, Houle S, Dozois CM, Bachman MA. 2016. *Klebsiella pneumoniae* siderophores induce inflammation, bacterial dissemination, and HIF-1α stabilization during pneumonia. mBio 7:e01397-16. https://doi.org/10.1128/mBio.01397-16
76. Wang J, Ji X, García P, Li J, Zhang L, Wang H, Wang R, He T. 2025. Evolution and transmission potential of *iuc3*-positive virulence plasmids in hypervirulent *Klebsiella pneumoniae*. Microbiol Res 299:128242. https://doi.org/10.1016/j.micres.2025.128242
77. Bachman MA, Oyler JE, Burns SH, Caza M, Lépine F, Dozois CM, Weiser JN. 2011. *Klebsiella pneumoniae* yersiniabactin promotes respiratory tract infection through evasion of lipocalin 2. Infect Immun 79:3309–3316. https://doi.org/10.1128/IAI.05114-11
78. Russo TA, Carlino-MacDonald U, Drayer ZJ, Davies CJ, Hutson A, Luo TL, Martin MJ, McGann PT, Lebreton F, Sanders A. 2025. Hypervirulent *Klebsiella pneumoniae* causing aortitis retains its capsule and mucoviscosity and remains genotypically and phenotypically stable over time. Res Sq:rs.3.rs-6740913. https://doi.org/10.21203/rs.3.rs-6740913/v1
79. Wantuch PL, Knoot CJ, Marino EC, Harding CM, Rosen DA. 2025. *Klebsiella pneumoniae* bioconjugate vaccine functional durability in mice. Vaccine (Auckl) 43:126536. https://doi.org/10.1016/j.vaccine.2024.126536
80. Wantuch PL, Knoot CJ, Robinson LS, Vinogradov E, Scott NE, Harding CM, Rosen DA. 2023. Capsular polysaccharide inhibits vaccine-induced O-antigen antibody binding and function across both classical and hypervirulent K2:O1 strains of *Klebsiella pneumoniae*. PLoS Pathog 19:e1011367. https://doi.org/10.1371/journal.ppat.1011367
81. Feldman MF, Mayer Bridwell AE, Scott NE, Vinogradov E, McKee SR, Chavez SM, Twentyman J, Stallings CL, Rosen DA, Harding CM. 2019. A promising bioconjugate vaccine against hypervirulent *Klebsiella pneumoniae*. Proc Natl Acad Sci USA 116:18655–18663. https://doi.org/10.1073/pnas.1907833116
82. Anderson MT, Mitchell LA, Zhao L, Mobley HLT. 2017. Capsule production and glucose metabolism dictate fitness during *Serratia marcescens* bacteremia. mBio 8:e00740-17. https://doi.org/10.1128/mBio.00740-17
83. Favre-Bonte S, Joly B, Forestier C. 1999. Consequences of reduction of *Klebsiella pneumoniae* capsule expression on interactions of this bacterium with epithelial cells. Infect Immun 67:554–561. https://doi.org/10.1128/IAI.67.2.554-561.1999
84. Blumenkrantz N, Asboe-Hansen G. 1973. New method for quantitative determination of uronic acids. Anal Biochem 54:484–489. https://doi.org/10.1016/0003-2697(73)90377-1
85. Tipton KA, Rather PN. 2019. Extraction and visualization of capsular polysaccharide from *Acinetobacter baumannii*. Methods Mol Biol 1946:227–231. https://doi.org/10.1007/978-1-4939-9118-1_21
86. Schwyn B, Neilands JB. 1987. Universal chemical assay for the detection and determination of siderophores. Anal Biochem 160:47–56. https://doi.org/10.1016/0003-2697(87)90612-9
87. Payne SM. 1994. Detection, isolation, and characterization of siderophores, p 329–344. *In* Methods in Enzymology. Vol. 235. Academic Press.
88. Mey AR, Craig SA, Payne SM. 2012. Effects of amino acid supplementation on porin expression and ToxR levels in *Vibrio cholerae*. Infect Immun 80:518–528. https://doi.org/10.1128/IAI.05851-11
89. Simon EH, Tessman I. 1963. Thymidine-requiring mutants of phage T4. Proc Natl Acad Sci USA 50:526–532. https://doi.org/10.1073/pnas.50.3.526
90. Holmes CL, Wilcox AE, Forsyth V, Smith SN, Moricz BS, Unverdorben LV, Mason S, Wu W, Zhao L, Mobley HLT, Bachman MA. 2023. *Klebsiella pneumoniae* causes bacteremia using factors that mediate tissue-specific fitness and resistance to oxidative stress. PLoS Pathog 19:e1011233. https://doi.org/10.1371/journal.ppat.1011233